THE ASTROPHYSICAL JOURNAL, 470:336–348, 1996 October 10

MULTIWAVELENGTH OBSERVATIONS OF SHORT-TIMESCALE VARIABILITY IN NGC 4151. II. OPTICAL OBSERVATIONS[1]

S. KASPI,[2] D. MAOZ,[2] H. NETZER,[2] B. M. PETERSON,[3] T. ALEXANDER,[2] A. J. BARTH,[4] R. BERTRAM,[3,5] F.-Z. CHENG,[6] K. K. CHUVAEV,[7] R. A. EDELSON,[8] A. V. FILIPPENKO,[4] S. HEMAR,[2] L. C. HO,[4] O. KOVO,[2] T. MATHESON,[4] R. W. POGGE,[3] B.-C. QIAN,[9] S. M. SMITH,[3] R. M. WAGNER,[3,5] H. WU,[10] S.-J. XUE,[6] AND Z.-L. ZOU[10]

Received 1996 February 14; accepted 1996 May 1

ABSTRACT

We present the results of an intensive ground-based spectrophotometric monitoring campaign on the Seyfert galaxy NGC 4151 for a period of over 2 months, with a typical temporal resolution of 1 day. Light curves for four optical continuum bands and the Hα and Hβ emission lines are tabulated. During the monitoring period, the continuum at 6925 Å varied by ∼17% while the continuum at 4600 Å varied by ∼35%, with larger variations in the near-UV. The wavelength dependence of the variation amplitude also extends into the far-UV. The dependence in the 2700–7200 Å range can be explained by the different relative starlight contributions at different wavelengths, but the large variability at 1275 Å cannot be explained in this way. The continuum variability timescale is of order 13 days and is similar in all optical wavelength bands. No evidence of a time lag between the optical continuum and the UV continuum and emission lines was found. The Hα emission-line flux varied by ∼12%, with a gradual rise throughout the campaign. Its cross-correlation with the continuum light curve yields a lag of 0–2 days. The variations in the Hβ emission-line flux are ∼30% and lag the continuum by 0–3 days. This is in contrast to past results in which a time lag of 9 ± 2 days was found for both emission lines. This may be due to a different variability timescale of the *ionizing* continuum or to a real change in the broad-line region gas distribution in the 5.5 yr interval between the two campaigns.

Subject headings: galaxies: active — galaxies: individual (NGC 4151) — galaxies: Seyfert

1. INTRODUCTION

The Seyfert 1 galaxy NGC 4151 is one of the best studied active galactic nuclei (AGNs) because of its brightness and variability properties. It has been studied at many wavelengths, and its characteristics are well known (see, e.g., Peterson 1988). Several monitoring campaigns have shown variability timescales from a few hours in the hard X-ray regime (Yaqoob et al. 1993), to a few days in the ultraviolet (see, e.g., Clavel et al. 1990) and the optical (see, e.g., Maoz et al. 1991), and several months in the IR (Prestwich, Wright, & Joseph 1992).

NGC 4151 was selected by the AGN Watch consortium as a prime target for an intensive multiwavelength spectroscopic monitoring campaign. The campaign took place for 2 weeks in 1993 December, using the *Compton Gamma Ray Observatory*, the *Advanced Satellite for Cosmology and Astrophysics*, *ROSAT*, *IUE*, and many ground-based telescopes. Crenshaw et al. (1996, hereafter Paper I) describe the UV results from *IUE*. This paper presents the observations and results of the ground-based optical campaign. The high-energy results (*CGRO*, *ASCA*, *ROSAT*) are described by Warwick et al. (1996, hereafter Paper III), and a multiwavelength comparison is given by Edelson et al. (1996, hereafter Paper IV).

A primary goal of AGN monitoring has been to determine the size of the broad-line region (BLR; see Peterson 1993 for a review). Of the many ground-based variability studies of NGC 4151, the most intensive have been those of Antonucci & Cohen (1983) and Maoz et al. (1991). Antonucci & Cohen monitored NGC 4151 at approximately monthly intervals for over a year. They found that the continuum and broad lines varied on timescales shorter than their temporal resolution and deduced a BLR radius of less than ∼30 lt-days. For these data Gaskell & Sparke (1986) reported an Hβ lag of 0–7 days and Hγ lag of 5–9 days. These observations were also analyzed by Peterson & Cota (1988), who combined them with their own data and arrived at a BLR size of 6 ± 4 lt-days. Maoz et al.'s (1991) monitoring campaign lasted for a period of 8 months with a mean sampling interval of 4 days. Cross-correlation, deconvolution, and modeling applied to the data indicated a BLR size of 9 ± 2 lt-days. The *IUE* monitoring campaign described by Clavel et al. (1990) yielded a characteristic timescale of 4 ± 3 days from the response of the C IV λ1549 and Mg II λ2798 emission lines to the UV continuum.

In this paper, we present the results of 2 months of monitoring of NGC 4151 with a time resolution of ∼1 day. In

[1] This paper is dedicated to the memory of K. K. Chuvaev, who passed away during the course of this work.

[2] School of Physics and Astronomy and the Wise Observatory, The Raymond and Beverly Sackler Faculty of Exact Sciences, Tel Aviv University, Tel Aviv 69978, Israel.

[3] Department of Astronomy, Ohio State University, 174 W. 18th Avenue, Columbus, OH 43210.

[4] Department of Astronomy, University of California, Berkeley, Berkeley, CA 94720.

[5] Postal address: Lowell Observatory, 1400 W. Mars Hill Road, Flagstaff, AZ 86001.

[6] Center for Astrophysics, University of Science and Technology of China, 96 Jinzai lu, Hefei, Anhui 230026, China.

[7] Deceased, 1994 November 15.

[8] Department of Physics and Astronomy, University of Iowa, Iowa City, IA 52242.

[9] Shanghai Astronomical Observatory, Chinese Academy of Sciences, 80 Nandan lu, Shanghai 200030, China.

[10] Beijing Astronomical Observatory, Chinese Academy of Sciences, Zhongguancun, Beijing 100080, China.

§ 2, we describe the ground-based observations together with their reduction and calibration and present light curves for the continuum and the Hα and Hβ emission lines. In § 3, we carry out a time-series analysis of the data and briefly discuss the results. A summary is given in § 4.

2. OBSERVATIONS

2.1. *Data and Reduction*

The main effort of the ground-based monitoring campaign was carried out at the Wise Observatory in Israel, using the 1 m telescope. The last 2 hours of each night, for a period of over 2 months starting on 1993 November 14, were dedicated to the monitoring of NGC 4151. Spectroscopic observations were performed with the Faint Object Spectrographic Camera (Kaspi et al. 1995), using a 10″–wide slit and a 600 line mm^{-1} grism, yielding a dispersion of 2 Å $pixel^{-1}$. The spectral resolution was determined by the seeing, which was 2″–3″; combined with the instrument spatial scale of 0.″9 $pixel^{-1}$, the spectral resolution was ∼5 Å. Two different slits were used every night, each located at a different position in the telescope's focal plane. One slit produced spectra in the range ∼4150–6050 Å (hereafter the "B side"), and the other covered the range ∼5060–6990 Å (the "R side"). With this setup we were able to monitor both the Hα and the Hβ emission lines while a large part of the AGN continuum between them was observed through both slits. This produced two independent measurements of the 5100–6000 Å continuum, since the object was centered in each slit separately.

The spectrograph was rotated to include, together with the nucleus of NGC 4151, a field star ("star 1" of Penston, Penston, & Sandage 1971, P.A. = 156.°3) that served as a local standard. This technique of using a local comparison star is described in detail by Maoz et al. (1990, 1994) and produces high relative spectrophotometric accuracy.

For each of the B-side and R-side setups, we tried to obtain two or more consecutive exposures per night, with typical integration times of 15 minutes per exposure. The data were reduced by using standard IRAF routines with an extraction window of ∼13″. The NGC 4151/star ratios of consecutive exposures were compared to test for systematic errors. The ratios almost always reproduced to 0.2%–1.2% at all wavelengths. The few nights on which the ratios between exposures differed by more than 3.5% were discarded. (Only three nights had ratios between 1.2% and 3.5%.) The NGC 4151 and the star spectra from the consecutive exposures were co-added to improve the signal-to-noise ratio, and the resultant NGC 4151 spectrum was divided by an absorption-line–free, interpolated and smoothed version of the co-added stellar spectrum. This removes atmospheric absorption from the Seyfert spectrum and provides the relative flux calibration. This procedure resulted in one spectrum per setup per night. Absolute photometric calibration was achieved by multiplying the NGC 4151/star ratio by a smoothed, flux-calibrated spectrum of the comparison star, obtained on photometric nights by using known spectrophotometric standards.

The second data set was obtained by the Ohio State University (OSU) group with the Perkins 1.8 m telescope at the Lowell Observatory. NGC 4151 was observed for 10 nights between 1993 December 2 and 11 UT with the Boller & Chivens spectrograph through a 5″ slit at P.A. = 90°. Many exposures were taken each night with integration times of 2–3 minutes each, with a total integration time of several hours (in order to study the variations on timescales of minutes). The spectra covered the wavelength range ∼4480–5660 Å. The data were reduced by using standard IRAF routines. The individual spectra were co-added to produce three spectra for each night, which, after checking for agreement of 1% or less, were added into one spectrum per night.

The third data set that will be presented here was obtained with the Kast double spectrograph (Miller & Stone 1993) on the Shane 3 m reflector at Lick Observatory, using a 4″ slit that was aligned along the parallactic angle. This set consists of three epochs. Seven other data sets were obtained by other AGN Watch members, covering anywhere between one and eight nights. These will be discussed in the following section.

2.2. *Calibration*

A project of this scope requires the intercalibration of the various data sets into a single, consistent set. The method used for this intercalibration is based on the [O III] λλ4959, 5007 narrow emission lines, by requiring all spectra to have the same flux in these lines. There are various ways of achieving this objective. The one adopted here is based on the method of Peterson et al. (1994).

The Wise data set, being the largest, was chosen as the reference data set. The [O III] λλ4959, 5007 emission-line fluxes were measured between the observed wavelengths of 4952–5051 Å by summing the measured flux above a straight line passing between the average flux in the 6 Å interval on each side of this wavelength range. This kind of measurement was determined by Baribaud & Alloin (1990) to be optimal for the [O III] emission lines.

A second scaling method used is described by van Groningen & Wanders (1992). This method finds the optimum scaling factor, wavelength shift, and convolution factor of one spectrum with respect to a reference spectrum by slowly varying these parameters until the residuals of one or more nonvariable narrow lines in the difference between the two spectra are minimized. This resulted in spectra and light curves that confirmed but did not improve (in terms of the internal scatter within one data set) the results of the former method.

The mean flux of the two [O III] emission lines through the Wise apertures was found to be $\mathcal{F}_{[O\ III]} = 1.575 \times 10^{-11}$ ergs s^{-1} cm^{-2}, with a scatter of 1.1%. [This is consistent with Antonucci & Cohen's (1983) result of $(1.19 \pm 0.06) \times 10^{-11}$ ergs s^{-1} cm^{-2} for the [O III] λ5007 flux.] We consider this to be the accuracy of the comparison-star method. As a test, all B-side spectra were scaled so that their measured $\mathcal{F}_{[O\ III]}$ agreed with the above flux. No obvious differences appeared in the Wise light curves before and after the [O III] scaling, demonstrating the reliability of the comparison-star method. An attempt to scale all R-side spectra to the same [S II] λλ6716, 6731 emission-line fluxes yielded similar results. A comparison of the overlapping continuum bands between the R-side and the B-side spectra shows an agreement of ∼1% for almost all epochs.

All other data sets were scaled to match their [O III] line fluxes to the Wise $\mathcal{F}_{[O\ III]}$ by multiplying each spectrum by a factor $\mathcal{F}_{[O\ III]}/F([O\ III])_{obs}$, where $F([O\ III])_{obs}$ is the measured [O III] line flux of the spectrum. Light curves were then measured for the Hβ line and the 5100–5150 Å contin-

TABLE 1

FLUX SCALE FACTORS

Data Set	Point-Source Scale Factor φ	Extended Source Correction G (10^{-14} ergs s^{-1} cm^{-2} Å^{-1})
OSU.....	0.9558 ± 0.0027	-0.758 ± 0.018
Lick	0.9349 ± 0.0043	-1.103 ± 0.023
Wise	1	0

uum. These two light curves, which were obtained for each data set, were then intercalibrated with the Wise data set.

The intercalibration method (Peterson et al. 1994) is as follows: First, a point-source correction factor φ was defined by the equation

$$F(\mathrm{H}\beta) = \varphi F(\mathrm{H}\beta)_{\mathrm{obs}} , \quad (1)$$

where $F(\mathrm{H}\beta)_{\mathrm{obs}}$ is the Hβ line flux measured for each spectrum after scaling its [O III] line flux to agree with the Wise $\mathscr{F}_{[\mathrm{O\ III}]}$, and where $F(\mathrm{H}\beta)$ is the Wise Hβ flux from an observation that is close in time (see below). The φ-factor accounts for the fact that different apertures resulted in different amounts of light loss for the given point-spread function (which describes the surface brightness distribution of both the broad lines and the AGN continuum source) and the partially extended narrow-line region.

An additive correction was applied to allow for the different amounts of starlight admitted by different apertures. This correction, G, was defined by the equation

$$F_\lambda(5100) = \varphi F_\lambda(5100)_{\mathrm{obs}} - G , \quad (2)$$

where $F_\lambda(5100)_{\mathrm{obs}}$ is the continuum measured in the observed wavelength range 5100–5150 Å after the spectrum was scaled to have the Wise [O III] line flux, and where $F_\lambda(5100)$ is the contemporaneous Wise result.

A problem unique to this monitoring project is that NGC 4151 could be observed by ground-based telescopes for only $\sim$2 hr at the end of each night. (Because of *ROSAT* constraints, the campaign on this object, which has a right ascension of $\sim 12^{\mathrm{h}}$, was executed in December.) Thus no pairs of nearly simultaneous observations from different observatories (to determine the values of φ and G) could be

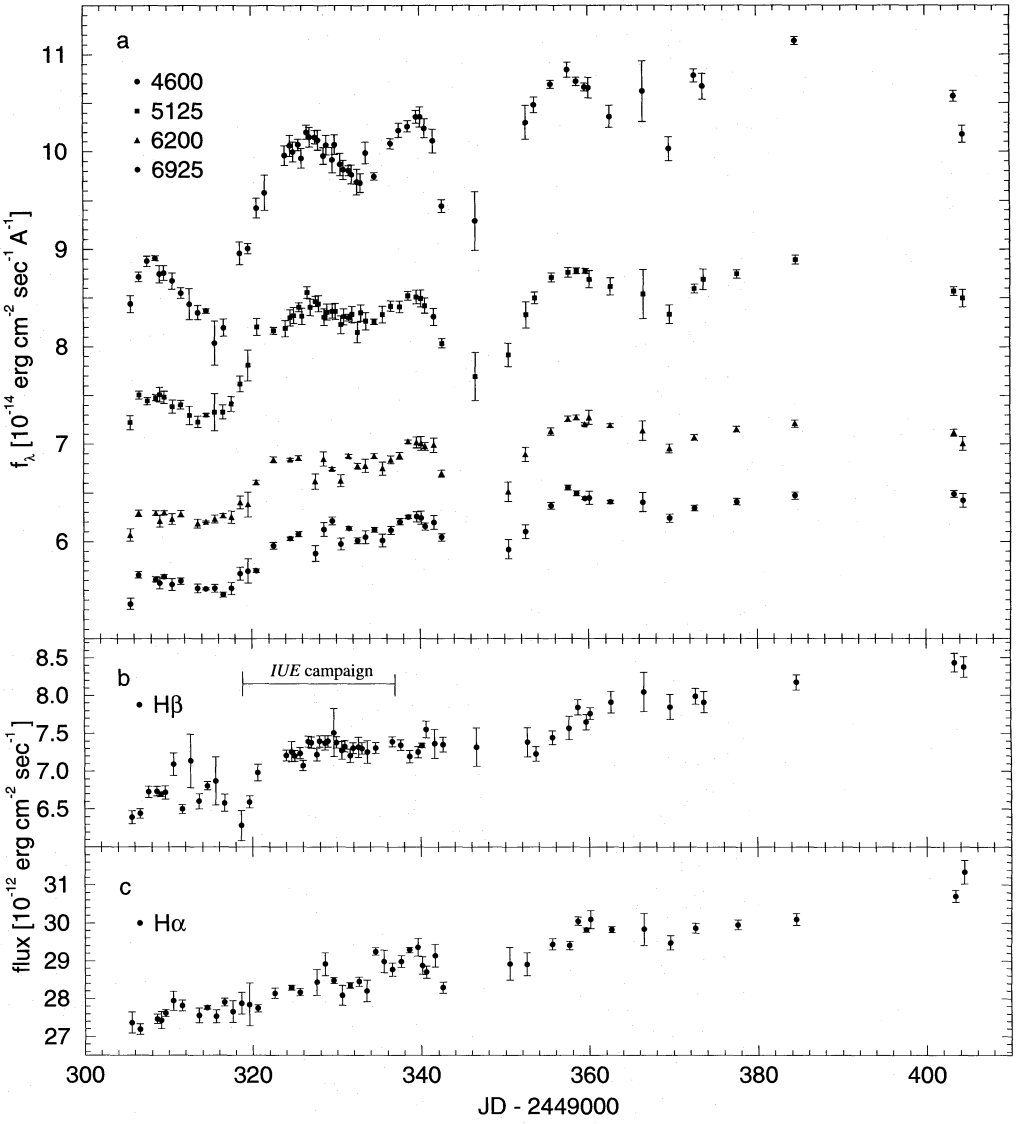

FIG. 1.—(*a*) Four optical continuum light curves for NGC 4151. Wavelength bands are listed in the upper left corner (in angstroms). The ordinate f_λ is given in absolute units. No shifts are applied to the top three light curves; the 6925 Å light curve is shifted by -5×10^{-15} ergs cm^{-2} s^{-1} Å^{-1}. (*b*) Hβ light curve. (*c*) Hα light curve.

TABLE 2

LIGHT CURVES

JD[a] (−2,449,000)	CONTINUUM FLUX (10^{-14} ergs cm^{-2} s^{-1} Å^{-1}) 4600 Å	5125 Å	6200 Å	6925 Å	EMISSION-LINE FLUX (10^{-12} ergs cm^{-2} s^{-1}) Hα	Hβ
305.6	8.44 ± 0.09	7.22 ± 0.07	6.07 ± 0.06	5.86 ± 0.06	27.36 ± 0.28	6.39 ± 0.09
306.6	8.72 ± 0.05	7.51 ± 0.04	6.29 ± 0.03	6.16 ± 0.03	27.20 ± 0.14	6.44 ± 0.06
307.6	8.88 ± 0.05	7.44 ± 0.04	...	...	...	6.73 ± 0.07
308.6	8.91 ± 0.03	7.48 ± 0.03	6.29 ± 0.03	6.11 ± 0.03	27.47 ± 0.12	6.74 ± 0.06
309.1[b]	8.75 ± 0.09	7.51 ± 0.08	6.21 ± 0.06	6.08 ± 0.06	27.43 ± 0.22	6.70 ± 0.03
309.6	8.76 ± 0.07	7.48 ± 0.06	6.30 ± 0.02	6.14 ± 0.02	27.62 ± 0.09	6.72 ± 0.09
310.6	8.68 ± 0.08	7.39 ± 0.07	6.23 ± 0.06	6.06 ± 0.06	27.94 ± 0.25	7.09 ± 0.15
311.6	8.55 ± 0.05	7.41 ± 0.05	6.28 ± 0.03	6.10 ± 0.03	27.81 ± 0.15	6.50 ± 0.06
312.6	8.44 ± 0.16	7.29 ± 0.09	...	...	...	7.14 ± 0.35
313.6	8.35 ± 0.07	7.23 ± 0.06	6.18 ± 0.04	6.02 ± 0.04	27.55 ± 0.20	6.60 ± 0.10
314.6	8.37 ± 0.02	7.30 ± 0.02	6.20 ± 0.01	6.02 ± 0.01	27.77 ± 0.05	6.81 ± 0.05
315.6	8.04 ± 0.23	7.33 ± 0.19	6.23 ± 0.04	6.02 ± 0.04	27.53 ± 0.17	6.87 ± 0.32
316.6	8.20 ± 0.09	7.33 ± 0.07	6.26 ± 0.02	5.96 ± 0.02	27.91 ± 0.10	6.58 ± 0.11
317.6	...	7.41 ± 0.08	6.25 ± 0.06	6.02 ± 0.06	27.66 ± 0.29	...
318.6	8.96 ± 0.12	7.62 ± 0.08	6.40 ± 0.07	6.17 ± 0.06	27.88 ± 0.28	6.29 ± 0.20
319.6	9.01 ± 0.05	7.81 ± 0.16	6.38 ± 0.13	6.20 ± 0.12	27.85 ± 0.56	6.60 ± 0.08
320.6	9.42 ± 0.10	8.20 ± 0.09	6.61 ± 0.02	6.20 ± 0.02	27.75 ± 0.10	6.98 ± 0.11
321.6	9.58 ± 0.18	...	...	...	...	...
322.6	...	8.16 ± 0.03	6.84 ± 0.03	6.46 ± 0.03	28.14 ± 0.13	...
324.0[c]	9.96 ± 0.10	8.19 ± 0.08	...	...	...	7.21 ± 0.07
324.6	10.06 ± 0.11	8.30 ± 0.09	6.84 ± 0.01	6.53 ± 0.02	28.28 ± 0.06	7.26 ± 0.13
325.0[c]	10.00 ± 0.10	8.32 ± 0.08	...	...	...	7.20 ± 0.07
325.6	10.07 ± 0.06	8.41 ± 0.04	6.86 ± 0.02	6.58 ± 0.03	28.17 ± 0.10	7.24 ± 0.07
326.0[c]	9.93 ± 0.10	8.31 ± 0.08	...	...	...	7.08 ± 0.07
326.6	10.20 ± 0.07	8.56 ± 0.06	...	...	...	7.39 ± 0.07
326.9[c]	10.15 ± 0.10	8.41 ± 0.08	...	...	...	7.38 ± 0.07
327.6	10.15 ± 0.07	8.47 ± 0.05	6.62 ± 0.08	6.38 ± 0.08	28.43 ± 0.34	7.22 ± 0.08
327.9[c]	10.12 ± 0.10	8.44 ± 0.08	...	...	...	7.40 ± 0.07
328.6	9.96 ± 0.08	8.30 ± 0.09	6.85 ± 0.07	6.63 ± 0.07	28.91 ± 0.30	7.37 ± 0.10
328.9[c]	10.07 ± 0.10	8.36 ± 0.08	...	...	...	7.40 ± 0.07
329.6	9.91 ± 0.13	8.37 ± 0.07	6.75 ± 0.02	6.71 ± 0.04	28.47 ± 0.08	7.51 ± 0.32
329.9[c]	10.07 ± 0.10	8.36 ± 0.08	...	...	...	7.38 ± 0.07
330.6	9.87 ± 0.11	8.23 ± 0.09	6.62 ± 0.06	6.47 ± 0.06	28.09 ± 0.26	7.27 ± 0.11
331.0[c]	9.81 ± 0.10	8.31 ± 0.08	...	...	...	7.33 ± 0.07
331.6	9.80 ± 0.05	8.30 ± 0.04	6.88 ± 0.02	6.63 ± 0.02	28.35 ± 0.07	7.21 ± 0.09
331.9[c]	9.77 ± 0.10	8.33 ± 0.08	...	...	...	7.31 ± 0.07
332.6	9.69 ± 0.13	8.15 ± 0.11	6.77 ± 0.03	6.51 ± 0.03	28.45 ± 0.12	7.32 ± 0.13
333.0[c]	9.68 ± 0.10	8.35 ± 0.08	...	...	...	7.30 ± 0.07
333.6	9.98 ± 0.11	8.26 ± 0.09	6.78 ± 0.07	6.55 ± 0.07	28.21 ± 0.29	7.25 ± 0.15
334.6	9.75 ± 0.04	8.26 ± 0.03	6.88 ± 0.02	6.62 ± 0.02	29.25 ± 0.10	7.31 ± 0.07
335.5	...	8.33 ± 0.09	6.75 ± 0.07	6.51 ± 0.07	28.99 ± 0.30	...
336.6	10.08 ± 0.05	8.42 ± 0.05	6.84 ± 0.04	6.62 ± 0.04	28.77 ± 0.18	7.39 ± 0.06
337.6	10.22 ± 0.07	8.41 ± 0.06	6.88 ± 0.04	6.70 ± 0.03	28.98 ± 0.15	7.35 ± 0.07
338.6	10.26 ± 0.06	8.52 ± 0.04	7.02 ± 0.02	6.75 ± 0.02	29.29 ± 0.07	7.20 ± 0.08
339.6	10.36 ± 0.07	8.51 ± 0.07	7.02 ± 0.06	6.75 ± 0.05	29.36 ± 0.24	7.25 ± 0.07
340.1[b]	10.36 ± 0.10	8.50 ± 0.08	7.01 ± 0.07	6.74 ± 0.07	28.88 ± 0.24	7.34 ± 0.03
340.6	10.24 ± 0.10	8.42 ± 0.08	6.98 ± 0.04	6.65 ± 0.04	28.70 ± 0.16	7.55 ± 0.11
341.6	10.11 ± 0.12	8.31 ± 0.09	6.99 ± 0.07	6.69 ± 0.07	29.13 ± 0.30	7.36 ± 0.19
342.6	9.44 ± 0.07	8.04 ± 0.05	6.70 ± 0.04	6.54 ± 0.04	28.29 ± 0.15	7.35 ± 0.10
346.6	9.29 ± 0.30	7.70 ± 0.25	...	...	...	7.32 ± 0.25
350.5	...	7.92 ± 0.12	6.51 ± 0.10	6.42 ± 0.10	28.92 ± 0.44	...
352.6	10.30 ± 0.17	8.33 ± 0.13	6.89 ± 0.07	6.60 ± 0.07	28.91 ± 0.30	7.38 ± 0.19
353.6	10.48 ± 0.08	8.50 ± 0.06	...	...	...	7.23 ± 0.10
355.6	10.69 ± 0.04	8.71 ± 0.05	7.13 ± 0.04	6.87 ± 0.04	29.44 ± 0.15	7.44 ± 0.09
357.6	10.84 ± 0.08	8.76 ± 0.05	7.26 ± 0.03	7.05 ± 0.03	29.41 ± 0.11	7.57 ± 0.15
358.6	10.72 ± 0.04	8.78 ± 0.03	7.28 ± 0.03	6.99 ± 0.02	30.05 ± 0.11	7.84 ± 0.10
359.6	10.66 ± 0.04	8.78 ± 0.02	7.20 ± 0.01	6.94 ± 0.02	29.82 ± 0.06	7.65 ± 0.10
360.1[b]	10.66 ± 0.11	8.70 ± 0.09	7.28 ± 0.07	6.95 ± 0.07	30.09 ± 0.24	7.76 ± 0.08
362.6	10.36 ± 0.11	8.62 ± 0.09	7.19 ± 0.02	6.91 ± 0.02	29.83 ± 0.08	7.91 ± 0.14
366.5	10.62 ± 0.31	8.54 ± 0.25	7.14 ± 0.10	6.90 ± 0.10	29.83 ± 0.42	8.05 ± 0.26
369.6	10.03 ± 0.12	8.34 ± 0.10	6.96 ± 0.04	6.74 ± 0.04	29.48 ± 0.19	7.85 ± 0.17
372.6	10.78 ± 0.07	8.60 ± 0.05	7.07 ± 0.03	6.84 ± 0.03	29.87 ± 0.13	7.99 ± 0.11
373.6	10.67 ± 0.13	8.69 ± 0.10	...	...	...	7.91 ± 0.14
377.6	...	8.75 ± 0.04	7.15 ± 0.03	6.91 ± 0.03	29.96 ± 0.13	...
384.6	11.14 ± 0.04	8.89 ± 0.05	7.21 ± 0.04	6.97 ± 0.04	30.10 ± 0.16	8.17 ± 0.10
403.4	10.57 ± 0.06	8.57 ± 0.04	7.12 ± 0.04	6.99 ± 0.04	30.71 ± 0.16	8.43 ± 0.12
404.4	10.18 ± 0.09	8.50 ± 0.09	7.00 ± 0.07	6.92 ± 0.07	31.34 ± 0.32	8.38 ± 0.14

[a] Observation Julian Date, rounded to a tenth of a day.
[b] Lick data.
[c] OSU data.

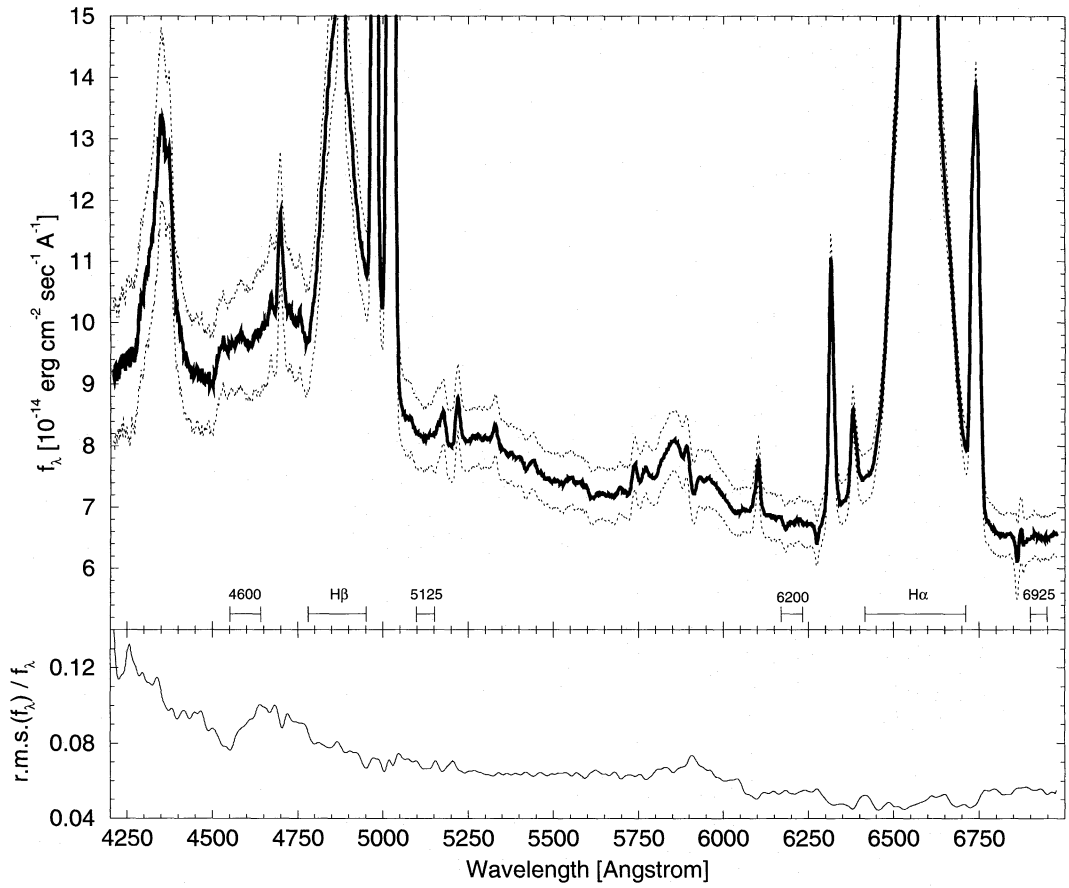

FIG. 2.—*Top*: Mean spectrum of NGC 4151 from the Wise data set. The dotted lines are the mean plus and minus the rms about the mean. Residual telluric features are visible at 6280 and 6860 Å. The continuum and line measurement bins are marked. *Bottom*: Smoothed ratio of the rms and the mean spectrum. The variation of the light curve's amplitude and its wavelength dependence can be seen from the larger variance at blue wavelengths.

found. This limits our ability to intercalibrate the various data sets and is different from previous monitoring campaigns (e.g., NGC 5548), in which objects could be observed all night and the time resolution was a few days.

Given the above difficulty, we have taken the alternative approach of interpolation. The reference Wise light curves of Hβ and F_λ(5100) were interpolated linearly, and for every spectrum in the other data sets, the values of F(Hβ) and F_λ(5100) at their precise date and time were found and used for defining φ and G (from eqs. [1] and [2]). The φ and G of each data set were then determined by averaging the values that were obtained for each spectrum of a data set. Finally, each spectrum of the given data set was multiplied by the average φ and G was subtracted, producing the final calibrated set.

The intercalibration constants, φ and G, for each data set are listed in Table 1. The φ for the OSU data set is in good agreement with its value as given by Peterson et al. (1995), who calculated it from the [O III] λ5007 surface brightness distribution of NGC 4151 through different apertures.

The intercalibration method can only be used for data sets with more than two epochs. Based on this criterion, several data sets had to be discarded. Also, all data sets with an internal accuracy worse than 3% (i.e., with spectra from the same night differing from each other, or from the Wise set, by more than 3%) were discarded. Given the small variation of the source during the period of intensive monitoring (1993 December 2–11), these data sets add no useful information and increase the overall noise.

In view of all these limitations, only the two large data sets from Wise and OSU, as well as the smaller Lick data set, will be discussed in the following sections.

2.3. *Line and Continuum Light Curves*

Figure 1*a* and Table 2 present mean continuum light curves for four spectral bands: (1) 4560–4640 Å (hereafter 4600 Å), (2) 5100–5150 Å (average of the Wise B side and R side and several points from the OSU and Lick sets, hereafter 5125 Å), (3) 6170–6230 Å (hereafter 6200 Å), and (4) 6900–6950 Å (hereafter 6925 Å). All wavelengths are in the observed reference frame. All four continuum light curves show the same feature of small "bumps" superposed on a gradual rise of the flux throughout the whole monitoring period. Examination of these light curves shows that the optical continuum changed (from a minimum at JD 2,449,315.6 to a maximum at JD 2,449,357.6) by $\sim$35% at 4600 Å and 17% at 6925 Å [$(F_{max}/F_{min}) - 1$]. This can also be seen in Figure 2 (*bottom*): the rms of the Wise light curves is $\sim$10% at 4600 Å whereas at 6925 Å it is $\sim$5%.

The Hβ flux was measured from each frame of the Wise B-side, OSU, and Lick sets, between the observed wavelengths 4780–4950 Å, by summing the measured flux above a straight line passing between the average flux in the intervals 4560–4640 and 5100–5150 Å. The Hα emission line was measured from the Wise R-side and Lick spectra between 6415 and 6710 Å, and its underlying continuum was measured between the average flux of two wavelength ranges 6170–6230 and 6890–6970 Å. Figure 1*b* and Table 2 show

the Hβ light curve, and Figure 1*c* and Table 2 show the Hα light curve. Both Hα and Hβ show a gradual rise in flux through the monitoring period, which amounts to $\sim$13% in Hα and $\sim$30% in Hβ. While, in the Hβ light curve, there are several features that resemble the continuum light curve (Fig. 1*a*), such features are barely visible in the Hα light curve.

3. ANALYSIS

3.1. *Cross-Correlations*

A main purpose of this and other monitoring campaigns is to measure the dimensions of the gas distribution in the BLRs of Seyfert galaxies. This is done by cross-correlating the line and continuum light curves and determining the time lag between them. Another goal is to study the variability properties of the sources. One of the methods we have applied to our data is the cross-correlation algorithm suggested by Gaskell & Peterson (1987). In this method, the cross-correlation function (CCF) is calculated twice for the two observed light curves $a(t_i)$ and $b(t_i)$: once by pairing the observed $a(t_i)$ with the interpolated value $b(t_i - \tau)$ and once by pairing the observed $b(t_i)$ with the interpolated value $a(t_i - \tau)$. The final CCF is taken to be the average of these two. No extrapolation was used, to avoid introducing artificial data, and the two last observed points of each light curve were omitted because of the large separation between them and the rest of the light curve. Linear and spline interpolation yielded similar results.

A major disadvantage of such interpolation methods is the lack of rigorous error estimates for the CCF and the deduced lag. One way to estimate the error is by assuming a certain BLR geometry and using simulations to find the significance of the measured lag (Maoz & Netzer 1989). Another way, suggested by Gaskell & Peterson (1987), is an analytic estimate for the uncertainty on the CCF peak position. This is only a rough estimate that relies on specific assumptions, such as uniform sampling of the data. We use it for lack of a better method.

An alternative way, which avoids interpolation, to find the CCF and the time lag with error estimates is to use the discrete correlation function (DCF; Edelson & Krolik 1988). The error estimate of this algorithm has been questioned by several authors (e.g., White & Peterson 1994; Paper IV). An improved algorithm was recently suggested by Alexander (1996). This new approach applies Fisher's *z*-transformation to the correlation coefficient and bins the DCF by equal-population, rather than equal-time, bins. It results in a more robust and statistically reliable method, the *z*-transformed discrete correlation function (ZDCF). The ZDCF peak position and its errors are estimated by a maximum likelihood method that takes into account the uncertainty in the ZDCF points.

Discrete binning implicitly assumes that the spacing between the data points is uncorrelated with their observing times. The NGC 4151 data treated here pose a special problem in this respect. The galaxy's sky position during this project allowed it to be observed only at the end of the night. As a result, most of the Julian Dates of the Wise set are at 0.6 of a day whereas most Julian Dates of the OSU set are at 0.0 day (Table 2). Since the OSU data only extend over one-eighth of the monitoring period, time lags of $n + 0.6$ days (where n is an integer), which cross-correlate OSU with Wise points, strongly depend on the behavior of the light curve during the OSU period whereas time lags of n days, which cross-correlate Wise with Wise points and OSU with OSU points, reflect the overall behavior of the light curve. This special sampling pattern resulted in spurious fluctuations between consecutive ZDCF points. Such fluctuations disappeared only when the ZDCF bin size was enlarged or when the OSU data were omitted from the light curves. Since the first option significantly decreases the number of ZDCF points, we use only the Wise data in the subsequent ZDCF time-series analysis. Below we present results from the ZDCF and the interpolated CCF methods (where data points from all sets were used). Both methods yield very similar results.

Table 3 shows the properties of the various CCFs calculated for the different continuum spectral bands. In this table, every wavelength band listed in a column is cross-correlated with every wavelength band listed in a row such that if the wavelength band in the row lags behind the wavelength in the column, then the time lag is positive. For every two bands, we calculated the CCF using the linear interpolation and the ZDCF methods. For each CCF, we

TABLE 3

CONTINUUM CCFs

	4600 Å		5125 Å		6200 Å		6925 Å	
CCF PROPERTIES	Linear	ZDCF	Linear	ZDCF	Linear	ZDCF	Linear	ZDCF
4600 Å:								
Time lag	0.0	0.0						
FWHM	11.0	10.0						
Peak correlation	1.00	1.00						
5125 Å:								
Time lag	$0.1^{+0.9}_{-0.9}$	$0.0^{+0.9}_{-0.8}$	0.0	0.0				
FWHM	11.5	12.5	13.6	14.4				
Peak correlation	0.97	0.96	1.00	1.00				
6200 Å:								
Time lag	$0.4^{+1.0}_{-1.0}$	$0.0^{+0.9}_{-0.6}$	$0.4^{+0.9}_{-0.9}$	$1.0^{+1.0}_{-1.6}$	0.0	0.0		
FWHM	11.7	10.5	11.9	11.3	11.4	12.3		
Peak correlation	0.96	0.95	0.97	0.97	1.00	1.00		
6925 Å:								
Time lag	$0.6^{+1.2}_{-1.2}$	$0.0^{+1.4}_{-0.5}$	$0.5^{+1.1}_{-1.1}$	$1.0^{+1.7}_{-1.2}$	$0.1^{+1.2}_{-1.2}$	$0.0^{+0.9}_{-0.6}$	0.0	0.0
FWHM	12.9	12.6	12.4	13.1	11.5	11.5	11.0	13.0
Peak correlation	0.97	0.95	0.96	0.96	0.98	0.97	1.00	1.00

NOTE.—See explanation in § 3.1.

list the time lag measured from the main peak, the error on the time lag (as described above), the FWHM of the main peak (measured at halfway between the peak's maximum and minimum), and the correlation coefficient of the peak. An example of a CCF of two continuum wavelength bands is given in Figure 3. The diagonal in Table 3 gives the autocorrelation function (ACF) results for all four continuum wavelength bands. The ACFs are plotted in Figure 4.

Table 4 lists the properties of the CCFs of the 5125 Å continuum light curve with the emission-line (Hα and Hβ) light curves, as well as the CCF of the emission lines with each other. This continuum band (which was observed in both the B side and the R side of the Wise set) was chosen since it is the most reliable one.

The Hα light curve (Figure 1*c*) shows a small, gradual rise of $\sim$12% throughout the entire campaign. No significant signal was found from cross-correlating it with itself. In contrast, the Hβ light curve (Fig. 1*b*) shows, on top of the gradual rise of $\sim$30%, in addition some features that follow the continuum variations. The CCFs of Hα and Hβ with the continuum light curve are illustrated in Figure 5.

3.2. *Continuum Variability*

Our monitoring of NGC 4151 for over 2 months with a temporal resolution of 1–4 days resulted in light curves with errors of 1% and can reveal variations as low as 3%. The variability timescale, defined as the FWHM of the main ACF peak (Table 3 and Fig. 4), is $\sim$13 days. The measured

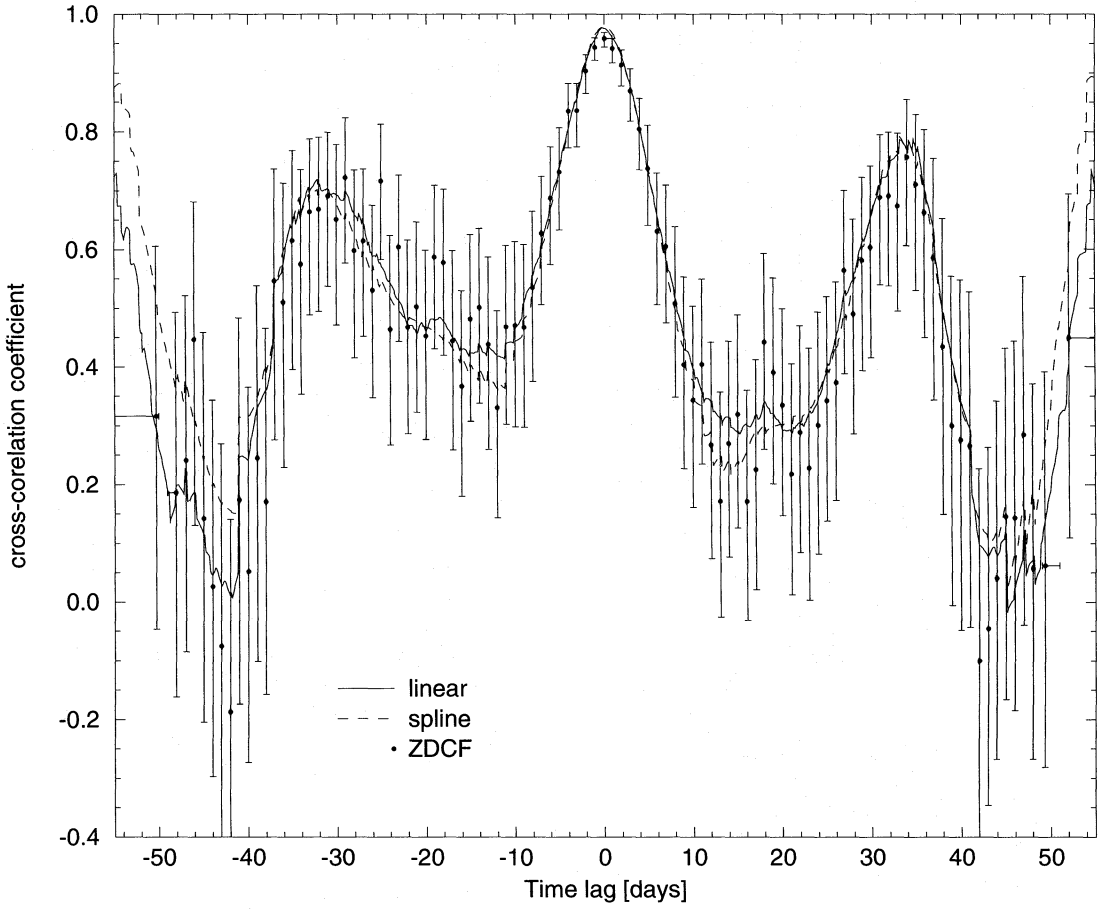

FIG. 3.—CCFs of two continuum wavelength bands, 4600 Å and 5125 Å, with linear interpolation (*solid line*), spline interpolation (*dashed line*), and ZDCF (*error bars with circles*). Note the good agreement between the three methods.

TABLE 4

EMISSION-LINE CCFs

	5125 Å		Hα		Hβ	
CCF Properties	Linear	ZDCF	Linear	ZDCF	Linear	ZDCF
Hα:						
Time lag.....	$0.6^{+1.7}_{-1.7}$	$1.0^{+5.0}_{-1.9}$	0.0	0.0		
FWHM.....	11.4	7.4	...	...		
Peak correlation.....	0.87	0.89	1.00	1.00		
Hβ:						
Time lag.....	$2.7^{+1.3}_{-1.3}$	$1.0^{+2.7}_{-1.2}$	$0.6^{+5.2}_{-5.2}$	$0.1^{+3.7}_{-11}$	0.0	0.0
FWHM.....	14.1	16.1	13.5	22.5	10.8	10.4
Peak correlation.....	0.88	0.83	0.90	0.83	1.00	1.00

NOTE.—See explanation in § 3.1.

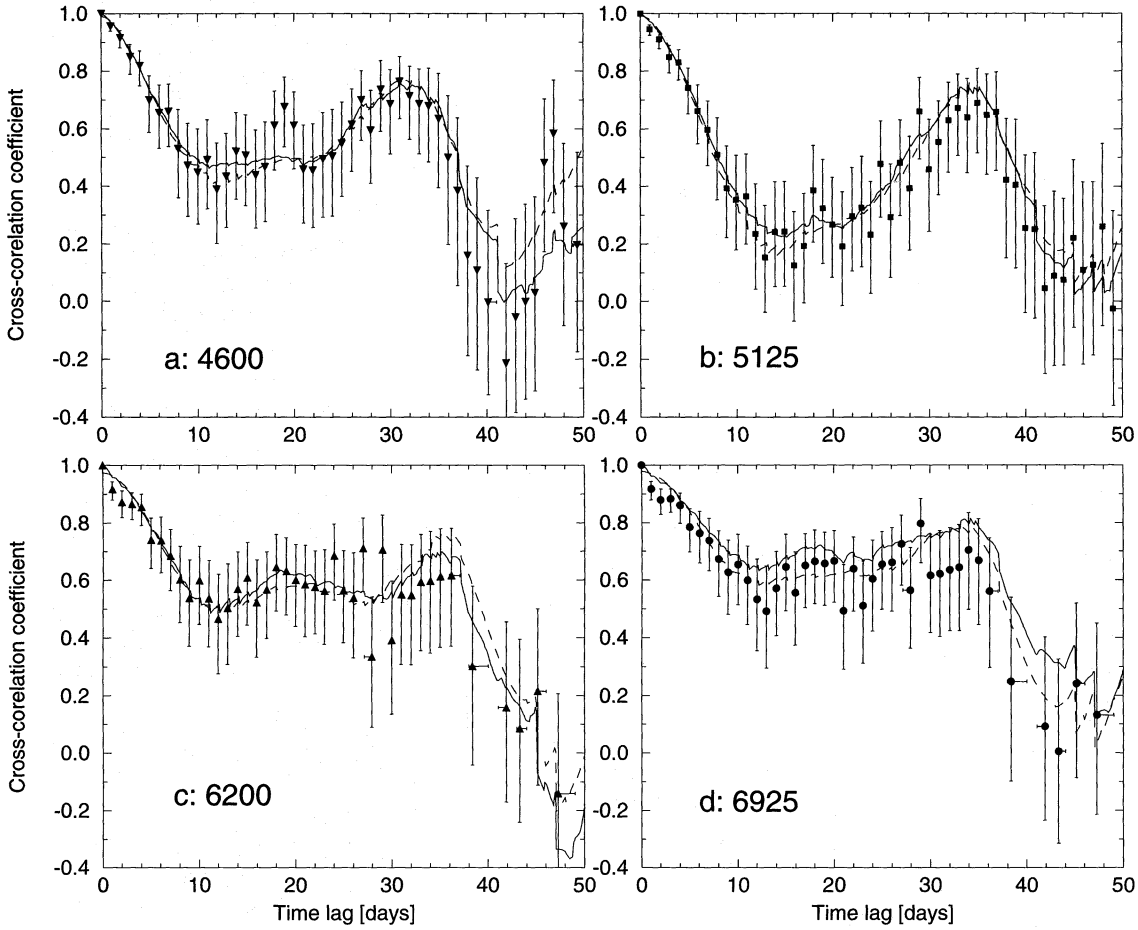

FIG. 4.—ACFs of the four continuum bands presented in Table 2. Notation is the same as in Fig. 3. (*a*) 4600 Å, (*b*) 5125 Å, (*c*) 6200 Å, and (*d*) 6925 Å.

continuum variations are 17%–35%, with amplitude decreasing toward longer wavelengths (Fig. 1*a*). This trend extends to shorter wavelengths, as can be seen by comparing the variability at UV wavelengths (Paper I) with the optical light curves presented here (Fig. 6). Figure 2, which shows the average and rms spectra of NGC 4151 from the Wise data set, illustrates this variable amplitude (see the larger variance at blue wavelengths in the bottom panel). Figure 7 presents this phenomenon in three dimensions: wavelength, Julian Date, and flux. Here we have made use of some more continuum wavelength bands, and the surface was interpolated over missing data points and smoothed.

To quantify the variability amplitude and its wavelength dependence, we calculated the power spectra of the four continuum light curves. Since the first 38 days of the monitoring period are evenly and almost regularly sampled by the Wise data set, it is reasonable to apply a discrete Fourier transform to these data. The power spectra are presented in Figure 8. The decreasing power of the variability with increasing wavelength is clear. A power-law fit, of the form PDS $\propto f^{\alpha}$, to the first six points yields an index α of -1.5 ± 0.9 for the wavelength bands 4600 and 5125 Å and -0.8 ± 0.6 for the wavelength bands 6200 and 6925 Å. The small variation amplitude, especially at the longer wavelengths, prevents us from determining a significant dependence of variation timescale on wavelength.

The dependence of the variability amplitude on wavelength can be explained by the varying relative contribution of starlight from the underlying galaxy. We show this by using template spectra of Sab galaxies from Coleman, Wu, & Weedman (1980) and Kinney et al. (1996). Based on previous observations of NGC 4151 (see Maoz et al. 1991), we estimate the galaxy's contribution to the spectrum through the Wise aperture, in the continuum wavelength band of 4600 Å, to be in the range (2–3.5) $\times 10^{-14}$ ergs cm^{-2} s^{-1} Å^{-1}. These numbers are confirmed by Peterson et al. (1995), who found the starlight contribution through the Wise aperture to be 2.2×10^{-14} ergs cm^{-2} s^{-1} Å^{-1}. We normalize the template spectra to these numbers and subtract the appropriate values from the four continuum light curves. When using the maximum value for the galaxy contribution at 4600 Å, we find that the relative change in each light curve during the 14 days of intensive monitoring is $\sim$20%, i.e., the differences in amplitude between the light curves presented in Figure 6 disappear. The 20% variation amplitude is also similar to that of the UV continuum at 2625–2750 Å (hereafter 2688 Å) but is different from that of the 1250–1300 Å (hereafter 1275 Å) light curve, where the relative variation is $\sim$35%.

We illustrate this result in Figure 9, where we present a simulation of the continuum light curves based on the 2688 Å continuum light curve. From the normalized galaxy template, we separated the total flux in this light curve into a galaxy contribution ($\sim$2%) and an AGN contribution ($\sim$98%). The resulting AGN light curve was scaled by a factor according to its part in the other wavelength ranges and was added to the galaxy contribution at each wavelength range. (The upper limit on the galaxy contribution at

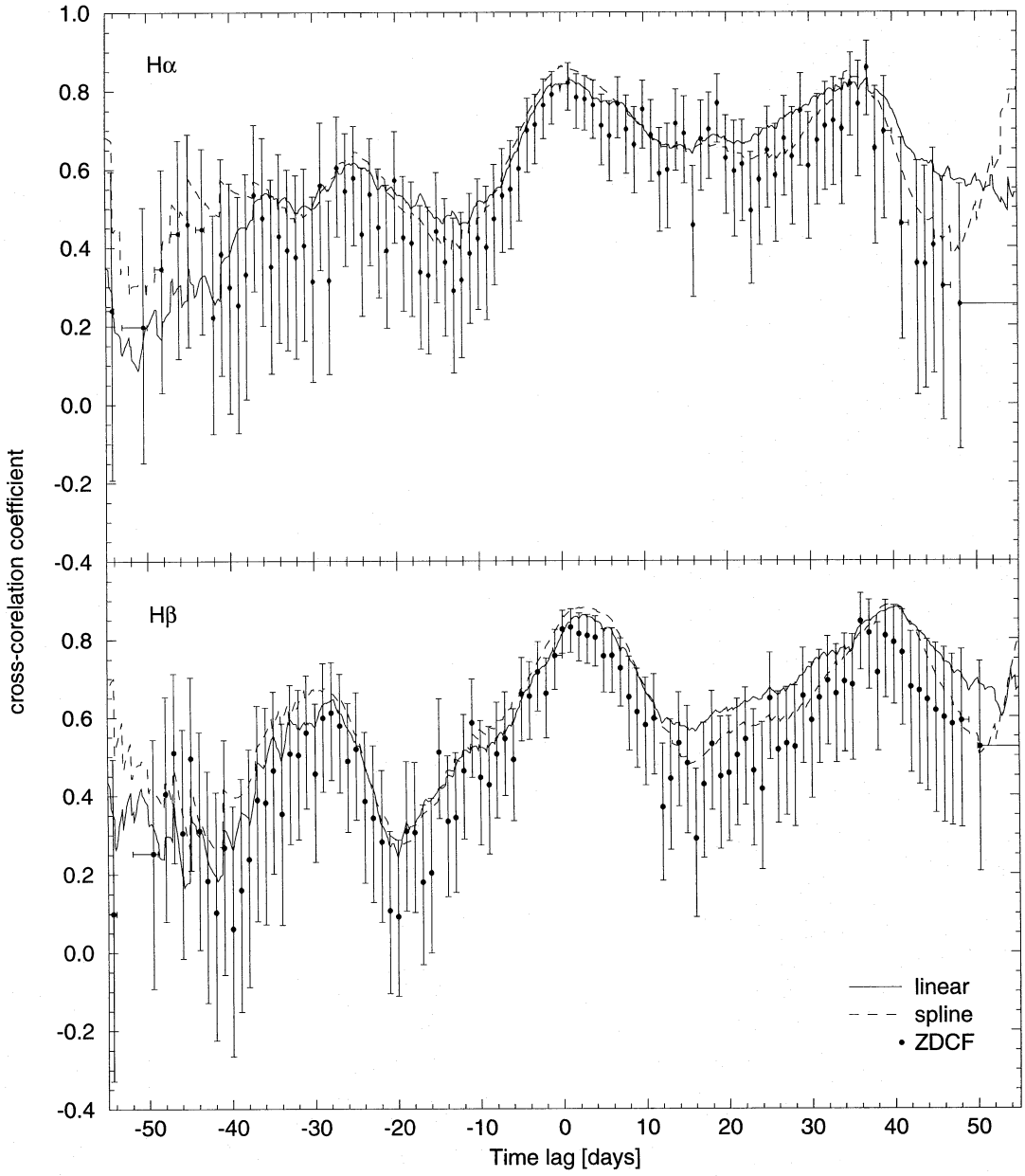

FIG. 5.—CCFs of the 5125 Å continuum band with Hα (*top*) and Hβ (*bottom*). Notation is the same as in Fig. 3. Note the time lag of ~ 0–3 days indicated by the main peak.

4600 Å, 3.5×10^{-14} ergs cm^{-2} s^{-1} Å^{-1}, gives the solid lines in Fig. 9, and the lower limit, 2×10^{-14} ergs cm^{-2} s^{-1} Å^{-1}, gives the dotted lines.) The observed data at all optical wavelengths show good agreement with the galaxy-diluted UV light curve. The wavelength dependence of the variability amplitude in the range 2700–7200 Å can thus be explained by the differing starlight contribution at different wavelengths. The 1275 Å UV continuum light curve's amplitude cannot be explained by use of the starlight contribution alone, as illustrated in the top panel of Figure 9.

From the CCFs of the different continuum wavelength bands with each other, no significant lags are detected, i.e., the continuum varies in phase at all optical wavelengths, to within 1 day. There is no apparent lag between the optical and UV light curves, as discussed in § 3.3 and in Paper IV.

No clear conclusions result from comparison of the optical light curves to the high-energy light curves (Paper III) since the high-energy monitoring period was brief compared to the optical variation timescale and the number of data points is relatively small.

3.3. *Emission-Line Variability*

The Hα light curve (Fig. 1*c*) shows a small, gradual rise throughout the entire campaign, and its ACF peak has a width of the duration of the program. No variability timescale can be deduced from this ACF. Cross-correlation of Hα with the 5125 Å continuum yields a time lag of 0–2 days (Fig. 5, *top*). The Hβ ACF indicates a variability timescale similar to that of the continuum (Table 4). Its CCF with the 5125 Å continuum (Fig. 5, *bottom*) suggests a lag with respect to the continuum light curve of 0–3 days. The CCF of the Hα and the Hβ light curves shows no lag, implying that both emission lines varied in phase.

We have performed cross-correlations of the UV continuum light curves (presented in Fig. 6) with the Hα and Hβ emission-line light curves. No significant time lags were

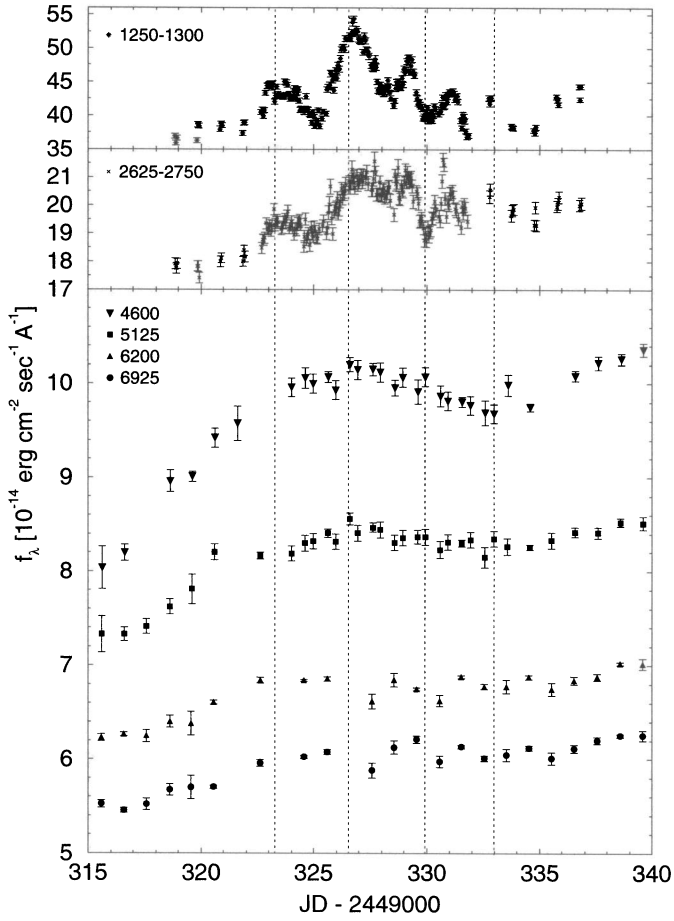

FIG. 6.—Same as Fig. 1*a*, but for the period of the *IUE* campaign. Two UV continuum light curves are shown for comparison with the optical continuum light curves.

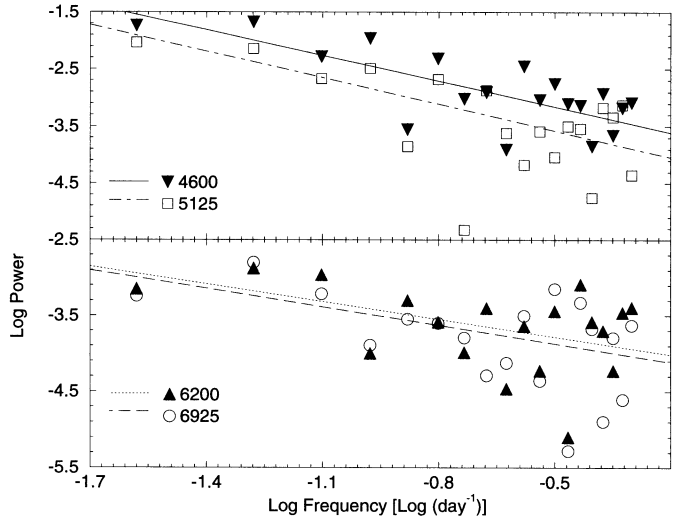

FIG. 8.—Power density spectra for the four continuum wavelength bands (calculated points and power-law fits). Note the decreasing power in variability with increasing wavelength.

found from these CCFs' peaks. The strong variations in the UV continuum light curves are of order 1–2 days, and such rapid variations were not detected in the optical emission-line light curves. This suggests a BLR size larger than 1–2 lt-days, in which light-travel time effects smear out the rapid variations of the ionizing continuum. Since no large-timescale variations (of order 10 days) took place during the UV monitoring period, no time lag between the UV light curves and the optical emission lines could be found.

Detailed analysis and cross-correlation of the optical light curves with the UV light curves (Paper I) for the *IUE* monitoring period are shown and discussed in Paper IV.

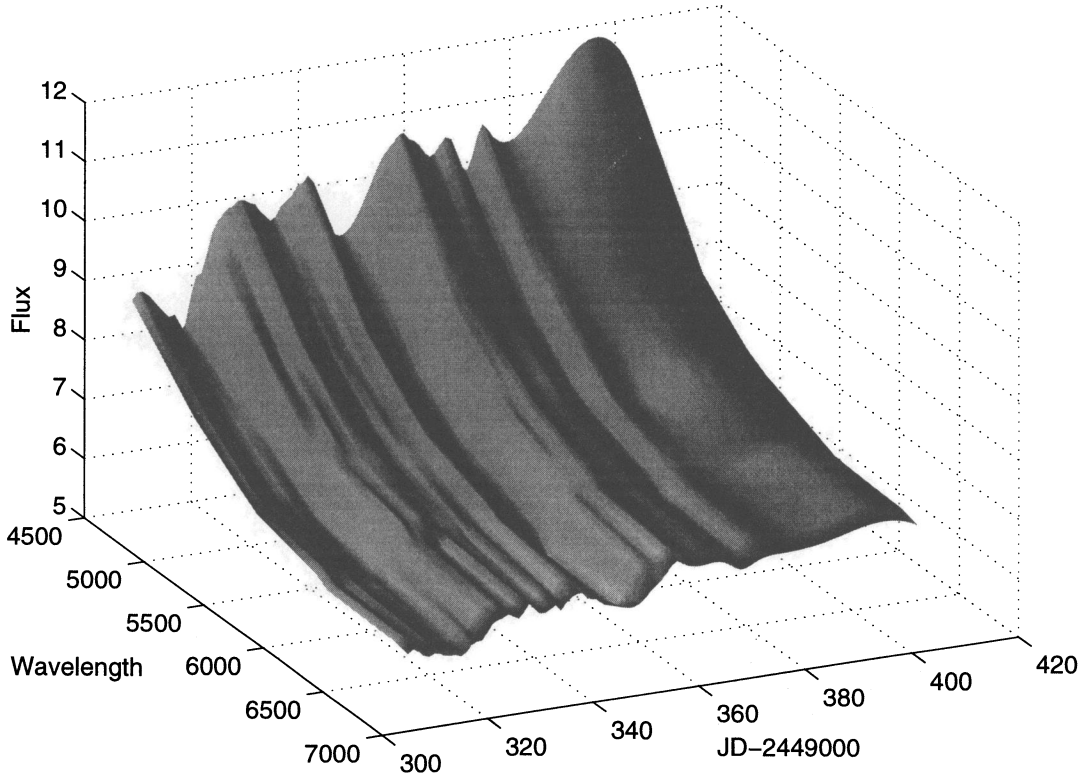

FIG. 7.—Continuum variability of NGC 4151. Wavelength is in angstroms, flux is in units of 10^{-14} ergs cm^{-2} s^{-1} Å^{-1}.

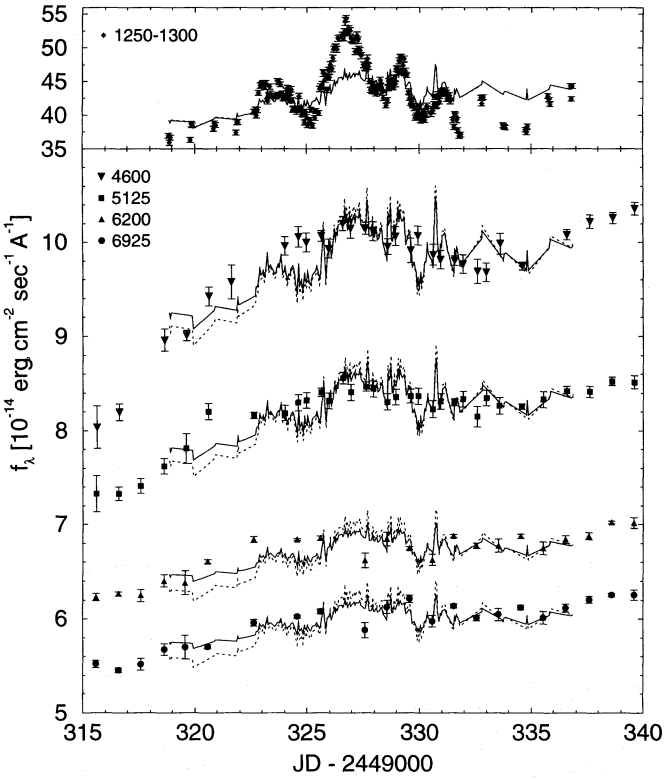

FIG. 9.—Light curves from Fig. 6 superposed on the linearly interpolated 2688 Å continuum light curve, after it was scaled and diluted with a constant starlight flux according to the galaxy contribution to the different wavelength bands: solid lines correspond to a galaxy contribution at 4600 Å of 3.5×10^{-14} ergs cm^{-2} s^{-1} Å^{-1}, and dotted lines correspond to a contribution of 2×10^{-14} ergs cm^{-2} s^{-1} Å^{-1}. Note the agreement between the scaled UV light curve and the optically observed points (*bottom*), indicating that the decrease in variability amplitude at larger wavelengths is mainly the result of dilution by the constant galaxy light. The 1275 Å UV light curve (*top*) is qualitatively different from the scaled 2688 Å light curve.

Here we discuss only the correlation of the UV light curve with the entire optical period, which includes 14 days of monitoring at the Wise Observatory, prior to the beginning of the *IUE* campaign.

Cross-correlation of the entire optical 5125 Å continuum light curve with the UV 1275 and 2688 Å continuum and the UV lines C IV λ1549 and He II λ1640 (Paper I) are shown in Figure 10. All three CCFs, of 2688 Å, C IV, and He II, show the same feature of a broad maximum, ranging from 0 to 6 days. We believe that this apparent positive delay is an artifact due to the finite duration of the monitoring campaign. This broad feature is probably a result of the optical continuum behavior prior to the UV monitoring: these three UV light curves show a gradual rise followed by period of constant flux, and the optical continuum light curve shows a gradual rise prior to the beginning of the UV monitoring. Those similar shapes result in high correlation ($\sim$0.8) over a period of a few days.

We have carried out two tests of this hypothesis. We have extrapolated the UV 2688 Å continuum to the period prior to the *IUE* monitoring based on the shape of the optical continuum. This was done by finding several 5125 Å continuum data points, that coincide in time with several 2688 Å continuum data points. The fluxes of these pairs of points were fitted with a linear function, which was then used to scale the 5125 Å light curve prior to the *IUE* campaign to the 2688 Å level. This extrapolated UV light curve was cross-correlated with the optical continuum and with the C IV line light curves, and yielded a CCF peak at zero lag. The second test is cross-correlation of the optical and UV light curves using only the part of the optical light curve that overlaps the *IUE* campaign. As shown and discussed in Paper IV (§ 3.4), the results are more narrowly peaked CCFs, consistent with a zero time lag. Thus both tests suggest that the time lags between the optical continuum and the UV line and continuum light curves are consistent with zero. The last conclusion explains the narrow-peaked (0–2 days) CCF of the 5125 Å continuum with the 1275 Å continuum, shown in Figure 10*a*. The lag and the difference between this CCF and others shown in Figure 10 are due to the fact that the 1275 Å continuum has more features in its light curve than the other UV light curves.

3.4. *Comparison with Past Results*

Maoz et al. (1991) monitored NGC 4151 in 1988 for a period of 8 months with an average sampling frequency of once every 4 days. They found continuum variations of $\sim$20%, similar to the 1993 amplitude, with a typical timescale of $\sim$28 days, about twice what is found in the present campaign ($\sim$13 days). They also found that both Hα and Hβ followed the continuum variations, and they were able to determine time lags of 9 ± 2 days with respect to the optical continuum for the two emission-line light curves. In this work, we find that the Hα and Hβ variations lag behind the optical continuum variations by 0–3 days. In both campaigns the Hβ response to the continuum variations is larger than the Hα response.

To investigate whether these discrepancies in emission-line lags are the result of the different continuum variability timescales or of different analysis methods, we have applied the autocorrelation methods described above to Maoz et al.'s (1991) data. We confirm that when using the interpolation methods (linear and spline) the variation timescale is $\sim$28 days. However, using the ZDCF, we find a variation timescale of $\sim$15 days. This difference can be explained by the fact that the 1988 monitoring program had several large gaps, which, when interpolated, increased the correlation between the continuum and line light curves at larger times. Using the data from the last 96 days of the 1988 campaign, which are more regularly sampled and have only one large gap, we find that both the interpolation and the ZDCF methods yield the same variability timescale of $\sim$15 days. NGC 4151 therefore had similar optical continuum variability behavior in 1988 and in 1993.

We have also performed cross-correlations of the emission lines and the continuum of the 1988 data. All cross-correlation methods yield the same results for the time lag, $\sim$8 days, consistent with the lag found by Maoz et al. (1991). The lag remains the same when only the last 96 points of the 1988 data are used. We conclude that the differences in Hα and Hβ lags behind the continuum between 1988 and 1993 are not the result of different methods of analysis.

Finally, we have checked by way of simulations whether the small lag we measure for the emission lines in 1993 could be the result of the particular form of the continuum variation in 1993, which consisted mainly of a monotonic rise. Assuming a spherical BLR shell of inner radius 2 lt-days and outer radius 30 lt-days (found by Maoz et al. to

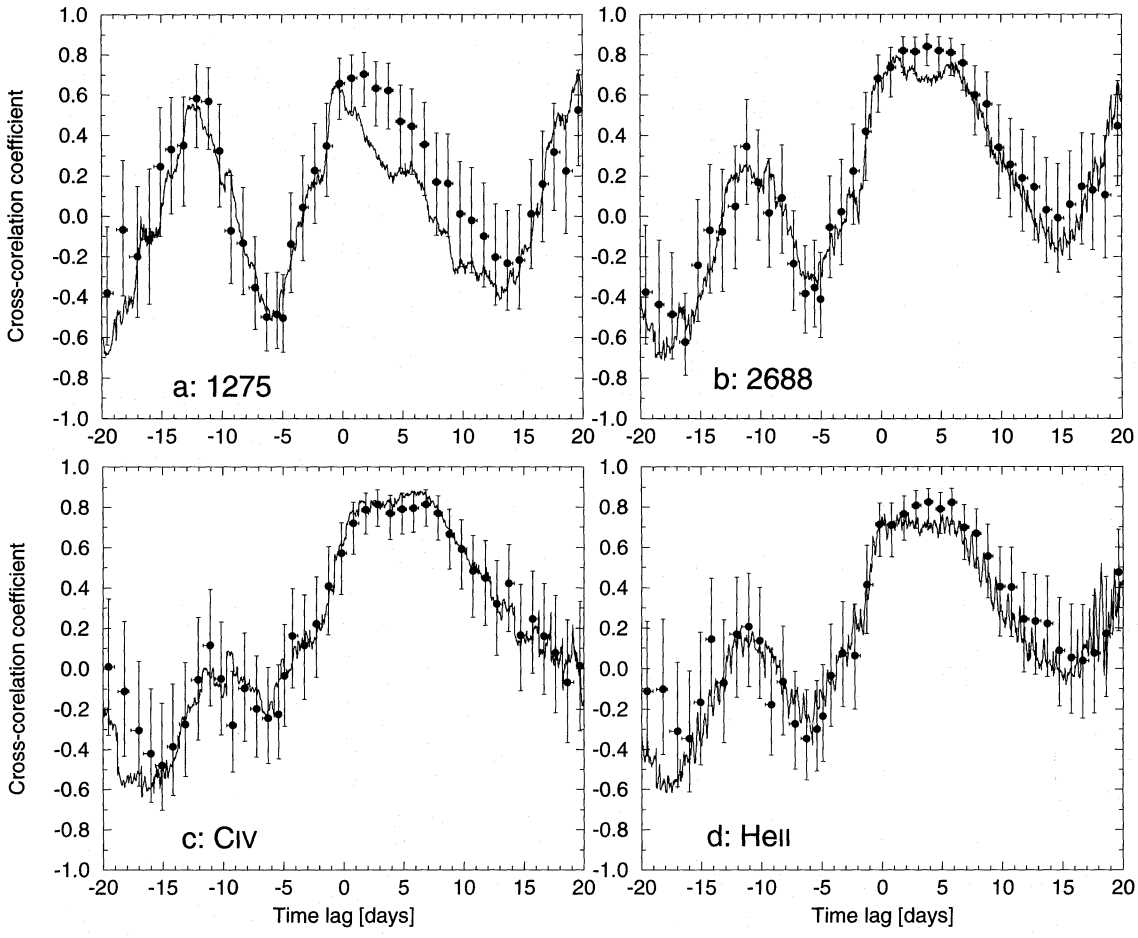

FIG. 10.—CCFs of the entire optical continuum 5125 Å band with the (*a*) 1275 Å UV continuum, (*b*) 2688 Å UV continuum, (*c*) C IV λ1549, and (*d*) He II λ1640. Notation is the same as in Fig. 3. The spline-interpolated CCF is not shown.

best fit their results), we calculated the emission-line light curve produced by such a geometry when driven by the spline-interpolated 4600 Å continuum light curve from the present campaign. We then sampled these two light curves at the same epochs of our actual observations and added to the sampled points a noise similar to the errors in our light curves. We applied to these light curves the various cross-correlation techniques discussed above and found the CCFs to have broad peaks at lags of ∼10 days. Thus the above thick-shell geometry, with an assumed ionizing continuum similar to the 4600 Å light curve of 1993, yields a lag that is much larger than that which we measure. The small time lags found in the 1993 data are probably not an artifact of the particular continuum behavior we observed.

If the above differences in emission-line lag are real, they may be related to the different state of NGC 4151, which, at the time of the 1993 campaign, was in an "active" state, in contrast to its lower flux level during the Maoz et al. monitoring campaign of 1988. (The optical continuum and line fluxes in the present monitoring campaign are about a factor of 2 higher than in 1988; see also Oknyanskij, Lyutyi, & Chuvaev 1994.) Evidence for a changing lag has been shown by Peterson et al. (1994) in the one other Seyfert galaxy that has been intensively monitored for several years, NGC 5548. A possible physical explanation for the change in the lag is a real change in the BLR gas distribution between 1988 and 1993. Such a change is, in principle, possible, considering the scales and velocities present in the nucleus of NGC 4151, which yield a dynamical timescale of ∼3 yr (see also Wanders 1994). An alternative explanation is that, during the present campaign, the optical continuum did not properly represent the behavior of the ionizing continuum. In particular, if the variability timescale of the *ionizing* continuum driving the lines is different between the two campaigns, the resulting time lags for the same BLR geometry can be very different (Netzer & Maoz 1990; Netzer 1991). Some evidence for this is seen in the differently shaped light curves of the 1275 and the 2688 Å continua (Fig. 9). This possibility is examined further in Paper IV.

4. SUMMARY

We have presented optical-band results of an intensive 2 month spectrophotometric monitoring campaign on the Seyfert galaxy NGC 4151, with a typical temporal resolution of 1 day. The main results of this campaign are as follows:

1. The continuum variations are between 17% and 35%, with decreasing amplitude toward longer wavelengths. The broad Hα line flux varied by ∼12% and the broad Hβ flux by ∼30%.

2. The decreasing continuum variability found at longer wavelengths can be explained by the varying contribution of starlight from the underlying galaxy. The exception to this is the far-UV 1275 Å continuum, where the variations must be intrinsically larger.

3. The various optical continuum bands vary in phase, with a lag of less than 1 day. The typical continuum variability timescale is ~ 13 days and is similar in all optical wavelength bands. The variability amplitude and timescale are similar to those observed in the past in this object.

4. No evidence of a time lag between the optical continuum and the UV continuum and emission lines was found. This may be partially the result of the short duration of the *IUE* campaign. Paper IV presents details on interband phase lags derived from the CCFs.

5. The Hα and Hβ light curves follow roughly the continuum variations and lag them by 0–3 days, in contrast to past results in which a time lag of 9 ± 2 days was found. This may be related to a different variability timescale of the *ionizing* continuum or to a real change in the BLR gas distribution in the 5.5 yr interval between the two campaigns.

We would like to thank P. Albrecht, M. Dietrich, J. Huchra, Yu. F. Malkov, S. L. Morris, V. I. Pronik, S. G. Sergeev, J. C. Shields, and B. J. Wilkes for contributing their data to this project. We are also grateful to John Dan, of the Wise Observatory staff, for his dedicated assistance with the observations. I. Wanders is thanked for providing his code for optimum [O III] scaling. The work of the University of California, Berkeley team was supported by NSF grant AST 89-57063 to A. V. F.

REFERENCES

Alexander, T. 1996, MNRAS, submitted
Antonucci, R. R. J., & Cohen, R. D. 1983, ApJ, 271, 564
Baribaud, T., & Alloin, D. 1990, A&A, 236, 346
Clavel, J., et al. 1990, MNRAS, 246, 668
Coleman, G. D., Wu, C. C., & Weedman, D. W. 1980, ApJS, 43, 393
Crenshaw, D. M., et al. 1996, ApJ, 470, 322 (Paper I)
Edelson, R. A., et al. 1996, ApJ, 470, 364 (Paper IV)
Edelson, R. A., & Krolik, J. H. 1988, ApJ, 333, 646
Gaskell, C. M., & Peterson, B. M. 1987, ApJS, 65, 1
Gaskell, C. M., & Sparke, L. S. 1986, ApJ, 305, 175
Kaspi, S., Ibbetson, P. A., Mashal, E., & Brosch, N. 1995, Wise Obs. Tech. Rep., No. 6
Kinney, A. L., Calzetti, D., Bohlin, R. C., McQuade, K., Storchi-Bergmann, T., & Schmitt, H. R. 1996, ApJ, 467, 38
Maoz, D., & Netzer, H. 1989, MNRAS, 236, 21
Maoz, D., et al. 1990, ApJ, 351, 75
———. 1991, ApJ, 367, 493
Maoz, D., Smith, P. S., Jannuzi, B. T., Kaspi, S., & Netzer, H. 1994, ApJ, 421, 34
Miller, J. S., & Stone, R. P. S. 1993, Lick Obs. Tech. Rep., No. 66
Netzer, H. 1991, in Lecture Notes in Physics, 377, Variability of Active Galaxies, ed. W. J. Duschl, S. J. Wagner, & M. Camenzind (Berlin: Springer), 107
Netzer, H., & Maoz, D. 1990, ApJ, 365, L5
Oknyanskij, V. L., Lyutyi, V. M., & Chuvaev, K. K. 1994, in IAU Symp. 159, Multi-Wavelength Continuum Emission of AGN, ed. T. J.-L. Courvoisier & A. Blecha (Dordrecht: Kluwer), 401
Penston, M. V., Penston, M. J., & Sandage, A. 1971, PASP, 83, 783
Peterson, B. M. 1988, PASP, 100, 18
———. 1993, PASP, 105, 207
Peterson, B. M., et al. 1994, ApJ, 425, 622
Peterson, B. M., & Cota, S. A. 1988, ApJ, 330, 111
Peterson, B. M., Pogge, R. W., Wanders, I., Smith, S. M., & Romanishin, W. 1995, PASP, 107, 579
Prestwich, A. H., Wright, G. S., & Joseph, R. D. 1992, ApJS, 80, 205
van Groningen, E., & Wanders, I. 1992, PASP, 104, 700
Wanders, I. 1994, in ASP Conf. Proc. 69, Reverberation Mapping of the Broad-Line Region in Active Galactic Nuclei, ed. P. M. Gondhalekar, K. Horne, & B. M. Peterson (San Francisco: ASP), 127
Warwick, B., et al. 1996, ApJ, 470, 349 (Paper III)
White, R. J., & Peterson, B. M. 1994, PASP, 106, 879
Yaqoob, T., Warwick, R. S., Makino, F., Otani, C., Sokoloski, J. L., Bond, I. A., & Yamauchi, M. 1993, MNRAS, 262, 435